https://doi.org/10.1595/205651322X16457018428071 *Johnson Matthey Technol. Rev.*, 2022, **66**, (4), 386–392

JOHNSON MATTHEY
TECHNOLOGY REVIEW

technology.matthey.com

3D-Printed Photoelectrochemical Cell and its Application in Evaluation of Bismuth Vanadate Photoanodes

Synthesis, cell design and testing

G. Kumaravel Dinesh, Paolo Dessì, Wenming Tong, Roberto González-Gómez, Pau Farràs*

School of Chemistry and Energy Research Centre, Ryan Institute, National University of Ireland Galway, University Road, Galway, Ireland, H91 TK33

***Email:** pau.farras@nuigalway.ie

PEER REVIEWED

Received 30th November 2021; Revised 23rd February 2022; Accepted 23rd February 2022; Online 24th February 2022

Bismuth vanadate ($BiVO_4$) is proven to be a promising photocatalyst for water splitting. However, the effect of materials syntheses, electrode preparation and size of photoelectrode on the photocurrent output of $BiVO_4$ photoanodes needs further investigations. In this study, three different $BiVO_4$ nanoparticle synthesis were employed, namely hydrothermal (HT), HT in the presence of ethylene glycol (EG) and HT with the addition of hydrazine hydrate (HH). In addition, two molecular inks (Triton-X and ethyl-methyl-imidazole, EMI), were compared for the preparation of $BiVO_4$ photoanodes using a simple doctor-blade technique followed by calcination at 450°C. The photoanodes (9 cm^2 active surface) were then compared for their photocurrent density at AM1.5G illumination and 1.2 V (*vs*. standard hydrogen electrode (SHE)) bias in a specifically designed, three-dimensional (3D)-printed electrochemical cell. The highest photocurrent 0.13 ± 0.1 mA cm^{-2} was obtained with the EMI ink, whereas tenfold lower photocurrent was obtained with Triton-X due to the higher charge transfer resistance, measured by electric impedance spectroscopy (EIS). The photoresponse was reproducible and relatively stable, with only 8% decrease in five consecutive illumination periods of 1 min.

Introduction

Sunlight-driven green hydrogen production is emerging as a promising contribution to carbon emission reduction, for which semiconductors as water splitting photocatalysts have arisen as potential materials to reach the worldwide climate goals at a low cost. As photoanode materials for oxygen evolution reaction (OER), bismuth-containing semiconducting metal oxides, such as $BiVO_4$, Bi_2WO_6 and Bi_2MoO_6, have shown convincingly visible-light-driven photocatalytic activities due to their well-matching band gaps and redox potentials of valence/conduction band positions (1). In particular, $BiVO_4$ demonstrated formidable photocatalytic performance for water splitting (2). However, $BiVO_4$ often suffers from fast recombination of the photogenerated electron-hole pairs, which limits the electron flow in photoelectrochemical cells (3).

$BiVO_4$ can be synthesised in various morphologies, sizes and crystal structures, which have direct impacts on their photocatalytic properties. It has traditionally been produced through solid-state processes, yielding fast-growing crystals with irregular morphologies and micron-scale sizes. Solution-based technologies, including aqueous,

HT and solvothermal processes, have been developed in recent years to synthesise various $BiVO_4$ nanostructures with improved charge transfer capabilities, such as nanoflakes, nanoellipsoids, nanowires, nanofibers, nanosheets, nanoplates and hyperbranched crystals (4–6). The size, shape and crystal structure of the $BiVO_4$ photocatalysts are closely linked to the synthesis conditions, including reaction media, pH value, temperature and reactant concentrations (7). Furthermore, the presence of surfactants or organic additives, such as HH (8) and EG (9), assists $BiVO_4$ formations with the desired polymorph. $BiVO_4$ photoanode films in working conditions suffer from leaching due to their low structural affinity to the electrode. The presence of inks, such as EMI and Triton-X, gives mechanical stability and better attachment to the film (10).

A plethora of $BiVO_4$ synthetic approaches and photoanode preparation methods are reported in the literature (8, 9, 11). The efficiency of such materials for hydrogen evolving photoelectrochemical cells is typically compared in terms of photocurrent densities generated, and by determining the overall solar-to-hydrogen (STH) and incident photon-to-current efficiencies (IPCE) (12), although in many cases the STH values are not correctly provided with no quantitative hydrogen measurement. In addition, a direct comparison of the photoelectrochemical performance is hampered by the different experimental conditions and cell design used in these reports. Standardising the experimental procedures, and in particular the cell design where the electrode materials are tested, is therefore necessary to enable a meaningful comparison of their photoelectrochemical performance.

In this study, a 3D-printed photoelectrochemical cell was purposely designed to allow a standardised comparison of the photocatalytic activity of $BiVO_4$-based photoanodes, further applicable to any other type of photoelectrode. The cell was employed to compare the photocurrent outputs of photoanodes produced using two different methodologies, namely doctor-blading and electrodeposition. For the doctor-blading approach, two inks (Triton-X and EMI) and $BiVO_4$ powders, synthesised in three different methods reported in the literature, namely HT with no additives, HT in the presence of EG and HT with the addition of HH, were mixed in various combinations to prepare the BVO_4 films on the photoanodes. A photoanode synthesised through a conventional electrochemical deposition method was used to demonstrate the greater extent of the designed cell. A thorough characterisation of the best performing photoanodes, including powder X-ray diffraction (XRD), scanning electron microscopy (SEM) and electric impedance spectroscopy (EIS), was performed to elucidate key differences affecting their photoelectrochemical behaviours.

Photoelectrochemical Cell Design

The test cell used in this study (**Figure 1** and Figure S1 in the Supplementary Information) was specifically designed to ensure a reproducible and standardised analysis of the photoanodes. The frame, which was 3D-printed in ultraviolet (UV)-cured resin materials, consisted of a base and a top part in a square shape (7×7 cm^2). The base had a chamber of approximately 20 ml volume hosting two fixed electrodes, a 2×2 cm^2 platinum-titanium mesh as the counter electrode and an Ag/AgCl reference electrode. Two holes were also included to introduce the electrolyte and allow operation in flow-cell mode. The top part was designed to host 5×5 cm^2 flat photoelectrodes and had a square window of 3×3 cm^2 to be exposed to illumination. The two parts were pushed onto each other through a rubber gasket by means of steel rods and plastic screws to ensure leak-proof adhesion of the electrode.

Photoanode Preparation and Testing

The $BiVO_4$ photocatalysts synthesised in various HT conditions are referred to as BVO-HT, BVO-HH and

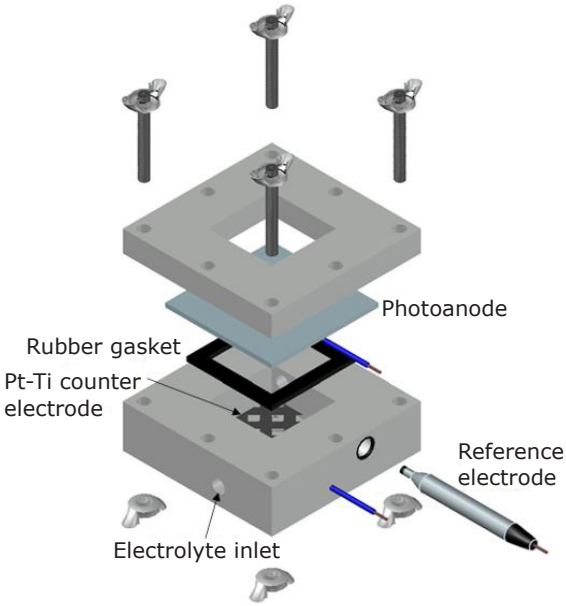

Fig. 1. Illustration of the design on a 3D-printed photoelectrochemical cell

BVO-EG, respectively, whereas the photocatalyst synthesised through the electrochemical deposition method is referred to as BVO-ED from now on. Each of the HT photocatalysts was first mixed with either Triton-X or EMI to form a colloidal paste, which was spread over a fluorine tin oxide (FTO) coated glass slide by doctor-blading technique to form a layer of 60 µm thickness and followed by calcination at 450°C in air, which ensures the formation of $BiVO_4$ in a uniform crystal structure. Higher calcination temperatures (500°C and 600°C) resulted in deteriorated photocatalytic activity (Figure S2 in the Supplementary Information) and were not further investigated. At lower calcination temperatures (<400°C), $BiVO_4$ exhibits a mixture of monoclinic and tetragonal crystal phases, which is not ideal for optimum photocatalytic activities (13), and the photoelectrode displays a dark residue due to the remaining ink that has not been calcined. The BVO-ED photoelectrode was prepared by electrodeposition of BiOI on the FTO followed by dropwise addition of vanadyl acetylacetonate and further calcination (14). The detailed synthetic methods, along with the photoanode preparation and testing methods are available in the Supplementary Information.

Three replicates of each photoanode were tested in the 3D-printed photoelectrochemical cell by linear sweep voltammetry (LSV) and chronoamperometry (CA) in 0.1 M phosphate buffer (pH 7) under dark and illuminated (AM1.5G) conditions. Prior to LSV analyses, each electrode underwent 3–6 cyclic voltammetry (CV) cycles for the same potential range until a stable profile was obtained. Among the photocatalysts synthesised with the HT method, LSV analyses (20 mV s^{-1} scan rate) showed a better photocurrent generation by the BVO-HH photoanodes prepared with both the Triton-X and EMI inks (**Figure 2(a)** and **(b)**). Therefore, BVO-HH based photoanodes became the focus of the study. The highest reproducible photocurrent of 0.44 ± 0.02 mA cm^{-2} was obtained with the BVO-HH-EMI at 1.8 V *vs.* SHE, whereas the current obtained under dark conditions (0.13 ± 0.02 mA cm^{-2}) was comparable to that of a bare FTO electrode (Figure S3 in the Supplementary Information), strongly suggesting the generation of higher current was due to the $BiVO_4$ photoanode film.

The photocurrent output of the BVO-HH photoanode was compared at 1.2 V *vs.* SHE in five alternate light/dark cycles of 60 s (**Figure 2(c)**). Significantly higher photocurrents were obtained using EMI ink (0.13 ± 0.01 mA cm^{-2}) rather than

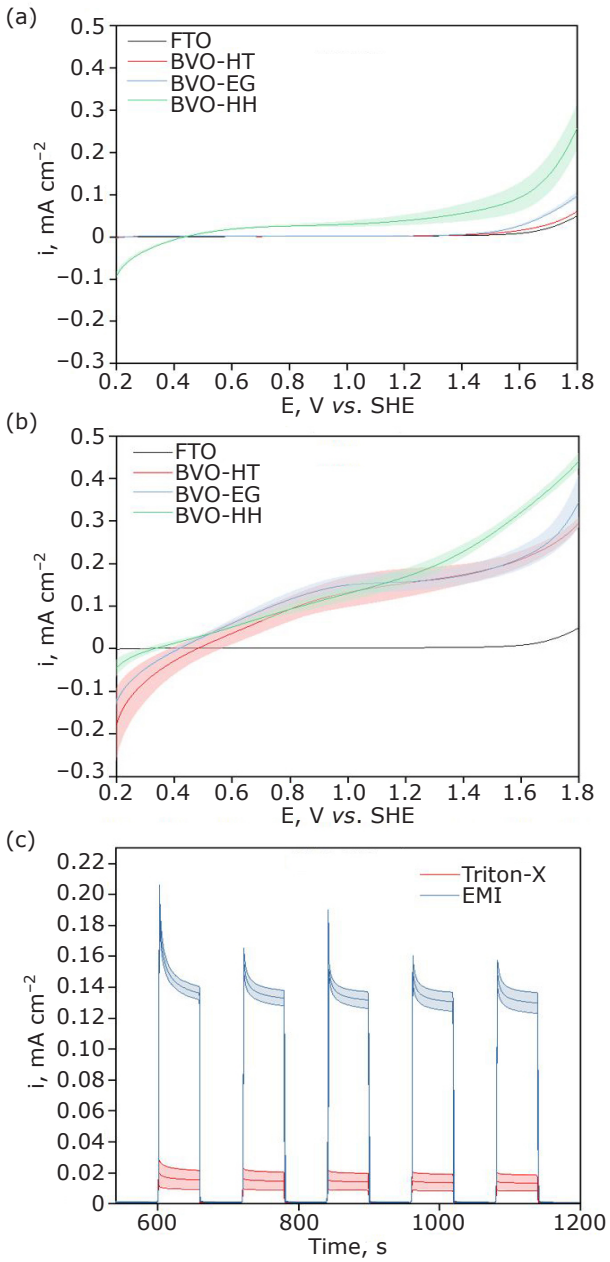

Fig. 2. LSV analyses under the illumination of the $BiVO_4$ photoanodes produced either with: (a) Triton-X ink; or (b) EMI ink; (c) CA analyses under the intermittent illumination of the BVO-HH electrodes at 1.2 V *vs.* SHE bias and AM1.5G illumination. The coloured lines and areas represent the average and interval of confidence of results obtained with three independent photoanodes

Triton-X (0.014 ± 0.005 mA cm^{-2}). The current output of the BVO-HH-EMI photoanode was twice higher than that obtained by the BVO-ED electrode (Figure S4 in the Supplementary Information), highlighting the potential of this synthesis method. It was also relatively stable over time, with 8.3% decay in the photocurrent after five consecutive illumination cycles (a total illumination period

for 300 s) against 15.9% decay of the electrode prepared with Triton-X ink.

A stability test was then performed using the same cell operated in flow-cell mode, where a phosphate buffer solution was constantly recirculated to the cell by a peristaltic pump. CA analyses under prolonged illumination resulted in an irreversible 78% drop of photocurrent in 24 h (Figure S5 in the Supplementary Information), which recovered neither after interrupting and resuming illumination nor after switching off the applied potential overnight and changing the electrolyte. Longer photocurrent stability (over 100 h) has been reported using potentiostatically photopolarised $BiVO_4$ electrodes (15), or sophisticated, multi-material photoanodes, such as plasma-etched NiOOH/$BiVO_4$ (16). The photocurrent output and stability are highly dependent on the $BiVO_4$ morphology and uniformity in the photoanode (17), which were thoroughly investigated by XRD, SEM and EIS measurements (**Figure 3**).

The XRD pattern of the as-synthesised $BiVO_4$-HH confirms the material is a mixture of monoclinic (Joint Committee on Powder Diffraction Standards (JCPDS) No: 14−0688) and tetragonal (JCPDS No: 14−0133) crystal structures. The corresponding SEM image shows the $BiVO_4$ synthesised through the HH method grew into a micro-spherical morphology with the diameter ranging from 2 µm to 7 µm (**Figure 3(a)**). A closer observation suggests these microspheres are assemblies of smaller particles. The calcination at 450°C during the preparation promoted a phase transition of tetragonal to monoclinic $BiVO_4$ for both photoanodes as indicated by the absence of tetragonal diffraction peaks (**Figure 3(e)**, BVO-HH-EMI and BVO-HH-Triton-X). In addition, two small diffraction peaks appeared at 27.3 and 27.9 degrees, implying the existence of a small quantity of monoclinic bismite Bi_2O_3 in both photoanodes. Compared to the as-synthesised $BiVO_4$-HH, calcinations in the presence of EMI or Triton-X both led to destruction of the microspheres into a coral-like porous structures as shown in their SEM images (**Figure 3(b)** and **3(c)**). This type of film structure is known to promote generation of photocurrent (18). The diameter

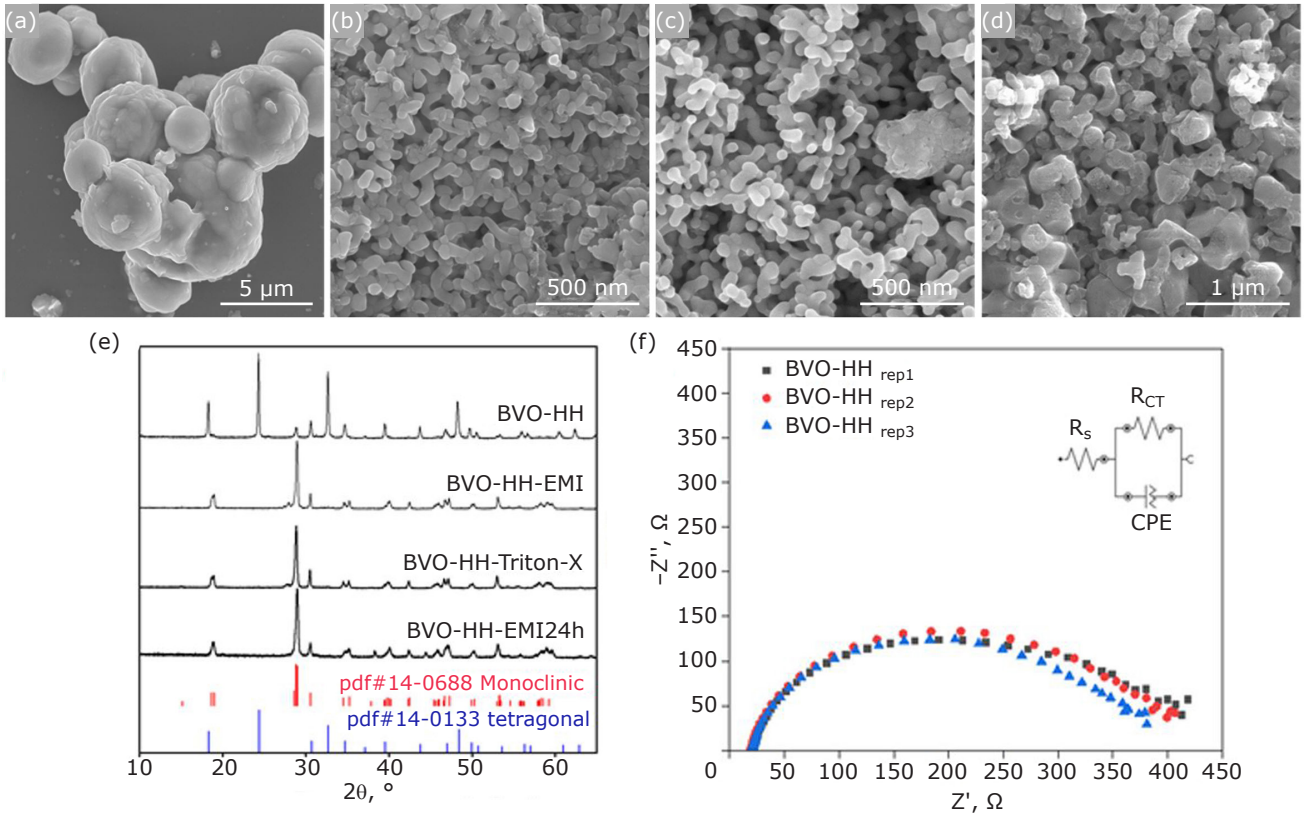

Fig. 3. SEM micrographs of the BVO-HH material: (a) as synthesised; (b) as deposited on the FTO glass electrodes after mixing with Triton-X followed by calcination; (c) as deposited on the FTO glass electrodes after mixing with EMI followed by calcination; (d) SEM micrograph of the BVO-HH-EMI material after the 24 h stability test; (e) respective XRD spectra of the materials; (f) Nyquist plot describing the impedance behaviour of the BVO-HH-EMI electrodes under illumination

of the 'coral-bone' is estimated to be ~120 nm for both photoanodes. The structure of the BVO-ED powder (Figure S6 in the Supplementary Information) was similar to the one obtained with the HT method after the calcination step, and XRD pattern (Figure S7 in the Supplementary Information) also confirms the presence of a monoclinic phase with small peaks of impurities. Thus, characterisations of the photoanodes so far gave very similar results and cannot explain the differences in the photoresponses in terms of morphological structure.

To get insights into the electron transfer mechanisms, the BVO-HH photoanodes prepared with either the Triton-X or EMI inks, as well as BVO-ED photoanode, were further analysed by EIS under illumination at an applied voltage of 1.2 V *vs.* SHE. A sinusoidal wave with 10 mV amplitude was applied in the frequency range from 0.1 Hz to 10^5 Hz (10 steps per decade). The results were visualised as Nyquist plot (**Figure 3(f)**, Figure S4 and Figure S8 in the Supplementary Information) and fitted to a Randles circuit to estimate ohmic drop, charge transfer resistance and pseudo-capacitance, as well as exponent of the constant phase element (CPE) (**Table I** and Table S2 in the Supplementary Information). The charge transfer resistance of the BVO-HH-EMI photoanode (330 ± 10 Ω) was one order of magnitude lower than that of the BVO-HH-TritonX (1700 ± 800 Ω), which correlates with the different photocurrent output of the two electrodes (**Figure 2**). It was also substantially lower than the charge transfer resistance of the BVO-ED photoanode (774 Ω). This suggests that the higher photocurrent output obtained with the EMI ink can be attributed to a more efficient electron transfer from the photocatalyst to the FTO electrode, and lower electron-hole recombination than with the Triton-X ink.

Table I Photoelectrochemical Parameters of the BVO-HH Electrodes Prepared with Triton-X or EMI Ink (Average and Standard Deviation of Triplicates)

Photoanode	R_S, Ω	R_{CT}, Ω	C, μF	α
BVO-HH-Triton-X	22 ± 3	1700 ± 800	140 ± 10	0.83 ± 0.04
BVO-HH-EMI	20 ± 1	330 ± 10	93 ± 3	0.81 ± 0.01

R_s = Ohmic resistance, R_{CT} = charge transfer resistance, C = pseudo-capacitance and α = exponent of the CPE

The origin of the conductivity disparity between the two HT BVO-HH-EMI and BVO-HH-Triton-X photoanodes might be highly related to the nature of the ink materials. EMI is a type of ionic liquid, which is much more conductive than Triton-X, a non-ionic surfactant. It was indeed previously postulated that the non-volatile imidazolium ring of EMI can help in increasing ionic conductivity and electrochemical stability (19). Therefore, it is plausible that very small amounts of the EMI or Triton-X were maintained in the thin films after the calcination process (10). This implies that it is possible to improve the conductivity of a photoanode by optimising the amount of EMI in future studies.

Furthermore, the electrodes prepared with EMI ink showed good reproducibility of the results (**Figure 3(f)**), whereas a high deviation was obtained for the electrodes prepared with Triton-X (Figure S8 in the Supplementary Information), particularly for the charge transfer resistance. The pseudo-capacitance of the photoanode prepared with EMI (93 ± 3 μF) was also lower than that obtained with Triton-X (150 ± 10 μF), resulting in a calculated electron lifetime of 0.03 ± 0.00 s and 0.2 ± 0.1 s, respectively. This further suggests that in the photoanodes prepared with EMI, the electrons spend a shorter time on the depletion layer of the semiconductor (20) and thus the probability of electron-hole recombination is lower than in the photoanodes prepared with Triton-X.

After the 24 h stability test, the XRD pattern of the $BiVO_4$ powder scratched off the BVO-HH-EMI contains additional diffraction peaks of unknown materials at 38.3 and 44.5 degrees (**Figure 3(e)**), suggesting the $BiVO_4$ within the photoanode has been partially decomposed due to the corrosion by the electrolyte solution and photoirradiation (21, 22). This, along with the gradual deconstruction of coral-like porous structure as shown in the corresponding SEM image (**Figure 3(d)**), account for the significant drop of the photocurrent during the 24 h prolonged stability run (Figure S5 in the Supplementary Information). In the case of for BVO-ED, SEM images were taken after the short-term photocurrent measurements (maximum of 20 min). The porous-like morphology of the as-prepared photoanode evolves to the formation of flower-like structures. The negligible atomic concentration of vanadium in the corresponding EDX results suggests these flower-like structures are bismuth oxide species (Figure S7 in the Supplementary Information).

This rapid degradation of the BVO photoanode is not observed even after the 24 h test done with the BVO-HH-EMI sample.

Conclusions

In conclusion, a photoelectrochemical cell was designed and 3D-printed to allow direct comparison of $BiVO_4$-based photoanodes. The $BiVO_4$ synthesised through the HH route (BVO-HH) gave the highest photocurrent output, and EMI outperformed Triton-X as ink for photoanode preparation due to its lower charge transfer resistance. The 3D-printed photoelectrochemical cell showed great robustness in measuring photocatalytic activities with its relatively easy experimental setup no matter its synthesis methodology as was demonstrated. The cell design can potentially be taken as a basic model for customisation, and most importantly, to standardise photocurrent measurements between different photoelectrode materials. The cell needs to be complemented by a protocol that can be replicated in different research laboratories. Further studies are required to improve photocurrent density (for example, by using co-catalysts such as cobalt phosphate) and stability in a long term (for example, adding protective layers), which is essential for industrial application.

Acknowledgements

This work was performed on the framework of the Science Foundation Ireland (SFI) Pathfinder Award on "Hybrid Bio-Solar Reactors for wastewater treatment and CO_2 recycling" (award nr. 19/FIP/ZE/7572PF). Wenming Tong and Pau Farràs acknowledge the financial support from INTERREG Atlantic Area programme (Grant reference EAPA_190_2016). Roberto González acknowledges financial support from INTERREG NPA programme (Grant reference 354). The SEM measurements in this work were performed in the Centre for Microscopy and Imaging at the National University of Ireland Galway, a facility that is funded by National University of Ireland Galway and the Irish Government's Programme for Research in Third Level Institutions, Cycles 4 and 5, National Development Plan 2007–2013.

References

1. X. Zhang, Z. Ai, F. Jia, L. Zhang, X. Fan and Z. Zou, *Mater. Chem. Phys*., 2007, **103**, (1), 77
2. T. Saison, N. Chemin, C. Chanéac, O. Durupthy, L. Mariey, F. Maugé, V. Brezová and J.-P. Jolivet, *J. Phys. Chem*. C, 2015, **119**, (23), 12967
3. C. Cheng, Q. Fang, S. Fernandez-Alberti and R. Long, *J. Phys. Chem*. Lett., 2021, **12**, (14), 3514
4. H. He, S. P. Berglund, A. J. E. Rettie, W. D. Chemelewski, P. Xiao, Y. Zhang and C. B. Mullins, *J. Mater. Chem. A*, 2014, **2**, (24), 9371
5. B.-C. Xiao, L.-Y. Lin, J.-Y. Hong, H.-S. Lin and Y.-T. Song, *RSC Adv*., 2017, **7**, (13), 7547
6. F. Q. Zhou, J. C. Fan, Q. J. Xu and Y. L. Min, *Appl. Catal. B: Environ.,* 2017, **201**, 77
7. R. A. Rather, A. Mehta, Y. Lu, M. Valant, M. Fang and W. Liu, *Int. J. Hydrogen Energy*, 2021, **46**, (42), 21866
8. M. Mousavi-Kamazani, *J. Mater. Sci.: Mater. Electron*., 2019, **30**, (19), 17735
9. S. Nikam and S. Joshi, *RSC Adv*., 2016, **6**, (109), 107463
10. E. A. Mohamed, Z. N. Zahran and Y. Naruta, *J. Mater. Chem*. A, 2017, **5**, (15), 6825
11. B.-X. Lei, L.-L. Zeng, P. Zhang, Z.-F. Sun, W. Sun and X.-X. Zhang, *Adv. Powder Technol.*, 2014, **25**, (3), 946
12. Z. Chen, H. N. Dinh and E. Miller, "Photoelectrochemical Water Splitting: Standards, Experimental Methods and Protocol", SpringerBriefs in Energy Series, Vol. 344, Springer Science and Business Media, New York, USA, 2013, 126 pp
13. M. F. R. Samsudin, S. Sufian, R. Bashiri, N. M. Mohamed and R. M. Ramli, *J. Taiwan Inst. Chem. Eng*., 2017, **81**, 305
14. K. R. Tolod, S. Hernández, M. Castellino, F. A. Deorsola, E. Davarpanah and N. Russo, *Int. J. Hydrogen Energy*., 2020, **45**, (1), 605
15. R.-T. Gao and L. Wang*, Angew. Chem. Int. Ed*., 2020, **59**, (51), 23094
16. R.-T. Gao, D. He, L. Wu, K. Hu, X. Liu, Y. Su and L. Wang, *Angew. Chem. Int. Ed*., 2020, **59**, (15), 6213
17. I. Khan, S. Ali, M. Mansha and A. Qurashi*, Ultrason. Sonochem*., 2017, **36**, 386
18. N. Kiama and C. Ponchio, *Surf. Coat. Technol*., 2020, **383**, 125257
19. A. Syairah, M. H. Khanmirzaei, N. M. Saidi, N. K. Ferhana, S. Ramesh, K. Ramesh and S. Ramesh, *Ionics*, 2019, **25**, (5), 2427
20. J. Ângelo, P. Magalhães, L. Andrade and A. Mendes, *Appl. Surf. Sci*., 2016, **387**, 183
21. D. K. Lee and K.-S. Choi, *Nat. Energy*, 2017, **3**, (1), 53
22. S. Zhang, I. Ahmet, S.-H. Kim, O. Kasian, A. M. Mingers, P. Schnell, M. Kölbach, J. Lim, A. Fischer, K. J. J. Mayrhofer, S. Cherevko, B. Gault, R. van de Krol and C. Scheu, *ACS Appl. Energy Mater*., 2020, **3**, 10, 9523

The Authors

G. Kumaravel Dinesh is working as a postdoctoral researcher at Ryan Institute, School of Chemistry, National University of Ireland Galway. He obtained his PhD in the Department of Chemical Engineering, National Institute of Technology Trichy, India, in 2016. His research work is mainly focused on nanomaterials for energy and environmental remediation, photocatalysis and photoelectrochemical studies of materials.

Paolo Dessì is the principal investigator of the SFI HyBioSol project and works as a postdoctoral researcher at Ryan Institute, School of Chemistry, National University of Ireland Galway. He holds a Masters degree in environmental engineering and a Marie Curie European joint PhD degree in environmental technology. His research focuses on the conversion of waste streams to valuable resources such as green chemicals and biofuels.

Wenming Tong is a postdoctoral researcher in ChemLight Group, School of Chemistry, National University of Ireland Galway. His research interests lie in the growths and optical properties of plasmonic nanoparticles, synthesis and characterisation of metal oxide nanoparticles, electrocatalysis and photocatalysis. He is closely associated with several projects within the research group, including European Union (EU) projects such as FlowPhotoChem, SEAFUEL and SOLAR2CHEM, as well as SFI HyBioSol project.

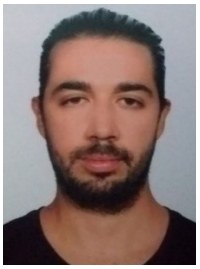

Roberto González Gómez is a postdoctoral researcher in the ChemLight group at National University of Ireland Galway with 9+ years' hands-on research experience and academic training. His research is focused on the synthesis and characterisation of nanoparticles for water oxidation. González is currently the workpackage leader of two EU-funded projects HUGE and NEFERTITI.

Pau Farràs is director of the ChemLight group, Lecturer in Inorganic Chemistry and Deputy Lead of the Energy Research Cluster at the Ryan Institute, at National University of Ireland Galway. Farràs is currently the coordinator of three EU-funded projects SEAFUEL, SOLAR2CHEM and FlowPhotoChem. He is co-author of 45 papers with over 1200 citations.

3D-Printed Photoelectrochemical Cell and its Application in Evaluation of $BiVO_4$ Photoanodes: Supplementary Material

*G. Kumaravel Dinesh, Paolo Dessì , Wenming Tong, Roberto González-Gómez, Pau Farràs**

School of Chemistry and Energy Research Centre, Ryan Institute, National University of Ireland Galway, University Road, Galway, H91 TK33, Ireland

Materials and methods

Reagents

$Bi(NO_3)_3•5H_2O$, NH_4VO_3, ethylenediamine and p-benzoquinone were purchased from Acros Organics. Ethylene glycol, hydrazine hydrate, Triton X-100, 1-ethyl-3-methylimidazolium trifluoromethanesulfonate (EMI) and vanadyl acetylacetonate were obtained from Fisher Scientific. Dimethyl sulfoxide (DMSO) was purchased from Fluorochem ltd. All chemicals were analytical grade and were used without further purification. Solutions were prepared using ultrapure MilliQ water.

Photoelectrode preparation – Hydrothermal method

$BiVO_4$ catalyst was synthesised following four different methods adapted from literature procedures. Three of them were hydrothermal approaches, where $BiVO_4$ was synthesised with only the bismuth and vanadium precursors (referred to as HT photoanode in the results) or with the addition of hydrazine hydrate (HH) or ethylene glycol (EG). In the HT method (1), $Bi(NO_3)_3•5H_2O$ (0.20 g, 0.44 mmol) and NH_4VO_3 (0.05 g, 0.43 mmol) were dissolved in a round bottom flask containing 100 mL of distilled water. As an alternative, 1 mL of ethylenediamine and 1 mL of hydrazine hydrate (80%) were added dropwise for the HH method (2). For the EG

Doi: 10.1595/205651322X16457018428071

method (3), $Bi(NO_3)_3 \bullet 5H_2O$ (0.25 g, 0.52 mmol) was dissolved in 5 mL ethylene glycol in continuous stirring. Then, NH_4VO_3 (0.06 g, 0.51 mmol) was added to the reactor and stirred until complete dissolution. The HT, HH and EG solutions were kept at 70 °C for 12 h and allowed to cool down to room temperature. For the EG method, 100 mL of distilled water were then added dropwise. The resulting yellow precipitates were collected and washed multiple times with distilled water and ethanol before drying at 70 °C under air for 10 h.

Fluorine tin oxide (FTO) electrodes (50 mm x 50 mm x 2.2 mm) (MSE supplies USA) were cleaned with acetone and allowed to dry at room temperature. Then the electrodes were fixed with adhesive tape leaving an uncovered surface of approximately 3 cm x 3 cm. Each $BiVO_4$ catalyst was mixed with 0.9 mL of either EMI (4) or Triton-X (5) to form a colloidal paste. The paste was spread over the FTO sheet by doctor-blading technique using an Elcometer (60 µm) and allowed to dry for a few minutes (< 5 min). The adhesive tape was then removed, and the electrodes were kept in a hot plate (Detlef Gestigkeit- model PR 5 3T) where the temperature was increased with a ramp rate of 5 °C·min^{-1} to 450 °C, kept stable for 15 min, and then cooled down to room temperature.

Photoelectrode preparation – Electrodeposition method

The fourth photoanode (ED) was prepared by electrodeposition (6). A 0.04 M $Bi(NO_3)_3$ in 0.4 M aqueous KI (pH 1.7) solution and a 0.23 M p-benzoquinone in absolute ethanol solution were prepared. Then, the solutions were mixed thoroughly at a Bi-KI to a benzoquinone-ethanol ratio of 1.9 to obtain the electrodeposition solution. The FTO electrode was cleaned by sonication for 15 min in acetone and MilliQ water. After, it was connected to the potentiostat as a working electrode, whereas a platinum mesh was used as the counter electrode and Ag/AgCl was the reference electrode. A potential of -0.1 V *vs* Ag/AgCl was applied for 90 min to deposit the BiOI on the electrode surface. Then, 0.4 M vanadyl acetylacetonate was prepared in DMSO, and 810 µL of that solution was drop casted on the FTO after 90 min to obtain $BiVO_4$. After dropcasting

the electrode was placed in hot plate and heated up to 450 ^{o}C (ramp rate of 5 ^{o}C·min^{-1}). Finally, the FTO was soaked in NaOH solution to wash out the excess vanadyl acetonante and dried at room temperature. The photos of electrode prepared through electrodeposition method are shown in Fig S9, the vanadyl acetylacetonate concentration and temperature ramp rate were optimised for the area of the electrode to obtain a homogenous film.

$BiVO_4$ photocatalyst characterisation

The X-ray diffraction (XRD) patterns of $BiVO_4$ were recorded on an Inel Equinox 6000 system with a 0.154056 nm Cu α-1 X-ray source. The morphologies of $BiVO_4$ were examined by a Hitachi S7400 scanning electron microscope. The photoelectrochemical properties were investigated using a Metrohm Autolab M204 potentiostat.

Photoelectrochemical cell set-up

The test cell used in this study (Figure S7) was specifically designed to ensure a reliable and replicable analysis of the photoelectrode. The frame, which was 3D printed in UV-cured resin material, consisting of a base and a top part square in shape (7 cm x 7 cm). The base had a chamber of approximately 20 mL volume hosting a 2 cm x 2 cm Pt-Ti mesh (Goodfellow, UK) as the counter electrode and an Ag/AgCl reference electrode (Alvatek, UK). Two more holes were also included to introduce the electrolyte and allow operation in flow-cell mode. The top part was designed to host 5 cm x 5 cm flat photoelectrodes and had a square hole of 3 cm x 3 cm to be exposed to illumination. The two parts were pushed on each other through a rubber gasket using steel rods and plastic screws to ensure leak-proof adhesion of the electrode.

Photoelectrode testing

The assembled cell was filled with approximately 20 mL of 0.1 M phosphate buffer containing 16.28 g·L^{-1} K_2HPO_4 and 0.88 g.L^{-1} KH_2PO_4 in ultrapure MilliQ water (pH 7, 23.3 mS·cm^{-1} conductivity) and placed below a solar simulator (Pico G2V Optics, US), providing a standard

Doi: 10.1595/205651322X16457018428071

AM1.5G light spectrum. The distance between the lens of the solar simulator and the photoelectrode was fixed at 3 cm, as set by the solar simulator calibration data. Each photoelectrode was tested, in triplicate, in three-electrode configuration by cyclic voltammetry (CV), linear sweep voltammetry (LSV) and chronoamperometry (CA) using an Uniscan PG580 potentiostat under both dark and illuminated conditions. Several CV cycles were performed in the potential range 0.2 - 1.8 V *vs* SHE (50 $mV \cdot s^{-1}$ scan rate) until a constant current response was obtained. Then, the LSV analyses were performed on the same potential range at 20 $mV \cdot s^{-1}$ scan rate.

The CA tests were performed at 1.20 V *vs* SHE by stabilising the electrode for 10 min under dark conditions, followed by five cycles of alternate illumination (1 min light and 1 min dark). CA was also applied to test the long-term response on the most performing electrodes. These tests were performed in flow-cell mode by continuously re-circulating 70 mL phosphate buffer from the cell to a glass bottle (kept slightly open to avoid overpressure) at a 12 $mL \cdot min^{-1}$ flow rate. The bottle was left open to avoid the accumulation of gas products during the tests. Selected photoelectrodes were also tested by electrical impedance spectroscopy (EIS) under dark and illuminated conditions using an Autolab M204 potentiostat (Metrohm, Switzerland) at an applied potential of 1.20 V *vs* SHE. The potential was chosen in a way that all the tested electrodes were photocatalytically active for the OER reaction (7). A sinusoidal wave with 10 mV amplitude was applied with a frequency range from 0.1 to 10^5 Hz (10 steps per decade). The experimental data were fit to a Randles circuit to estimate ohmic drop, charge transfer resistance and pseudo-capacitance. All results were validated for causality, linearity and stability by applying the Kronig-Kramer test.

Doi: 10.1595/205651322X16457018428071

Supplementary table

Table S1 – Comparison of $BiVO_4$ photoanode performance using different synthesis methods, all tested at 100 $mW \cdot cm^{-2}$. Photocurrent values obtained using chromoamperometry measurements.

Method	Photocatalyst	Potential applied	Electrolyte	Photocurrent ($mA \cdot cm^{-2}$)	Ref
Electrodeposition	$Bi/BiVO_4$	0.80 *vs* RHE	Sodium sulfate buffer (pH 7.35)	0.40	8
Spin coating	$F:BiVO_4@Ar$	1.23 *vs* RHE	Sodium sulfate buffer (pH 6.80)	1.15	9
Hydrothermal	$F:FeOOH/BiVO_4$	1.23 *vs* RHE	Sodium sulfate buffer (pH 7.35)	2.70	10
Hydrothermal	$BiVO_4$	1.20 *vs* SHE	Phosphate buffer (pH 7.00)	0.13	**This work**
Electrodeposition	$BiVO_4$	1.20 *vs* SHE	Phosphate buffer (pH 7.00)	0.06	**This work**

Table S2. Photoelectrochemical parameters of the BVO-ED and BVO-HH electrodes prepared with Triton-X or EMI ink (average and standard deviation of triplicates). Ohmic resistance (R_S); charge transfer resistance (R_{CT}); pseudo-capacitance (C) and exponent (α) of the CPE. BVO-ED measurements done in one photoelectrode.

Photoanode	R_S (Ω)	R_{CT} (Ω)	C (μF)	α
BVO-HH-Triton-X	22 ± 3	1700 ± 800	140 ± 10	0.83 ± 0.04
BVO-HH-EMI	20 ± 1	330 ± 10	93 ± 3	0.81 ± 0.01
BVO-ED	24	774	80	0.89

Doi: 10.1595/205651322X16457018428071

Supplementary figures

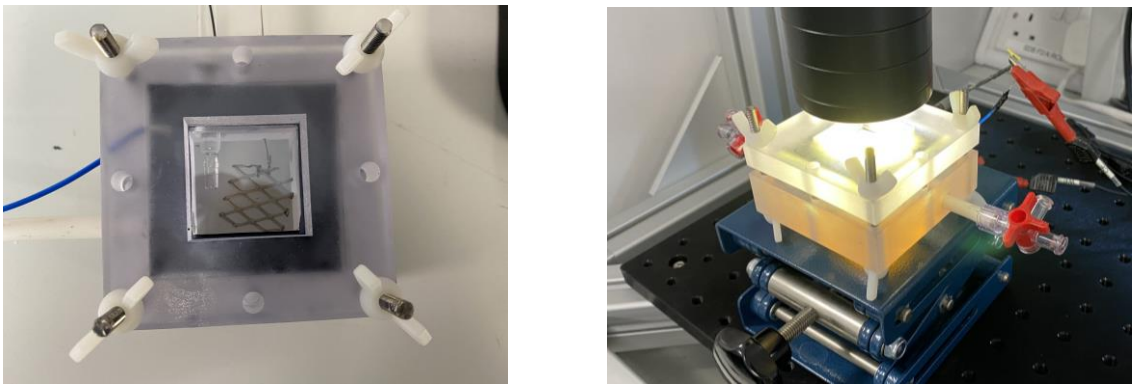

Fig. S1 – (left) Top view of the photoelectrochemical cell, using an FTO electrode; (right) photoelectrochemical cell in operation illuminated using a Pico G2V Optics solar simulator, located at 3 cm distance from the lens.

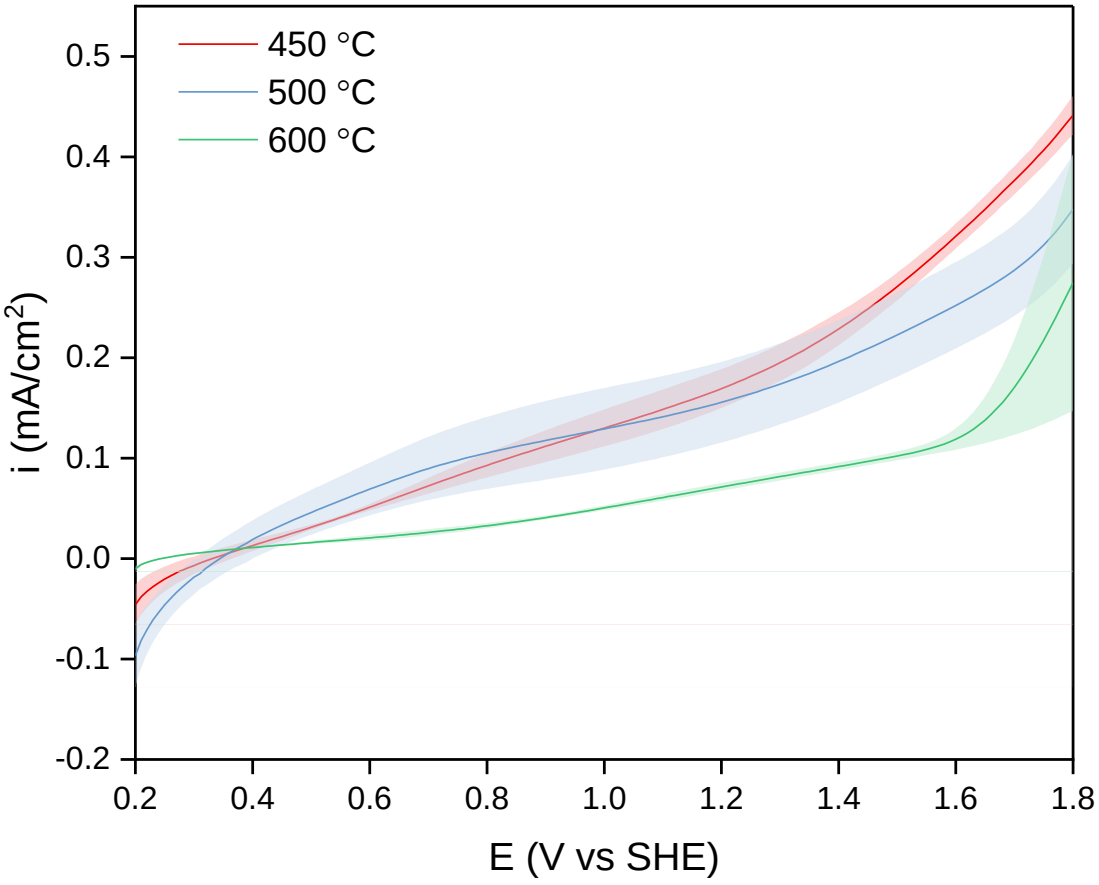

Fig. S2 – LSV analyses of the BVO-HH photoanodes produced with EMI ink at different annealing temperatures under AM1.5G illumination. The coloured lines and areas represent the average and interval of confidence obtained with three independent photoanodes.

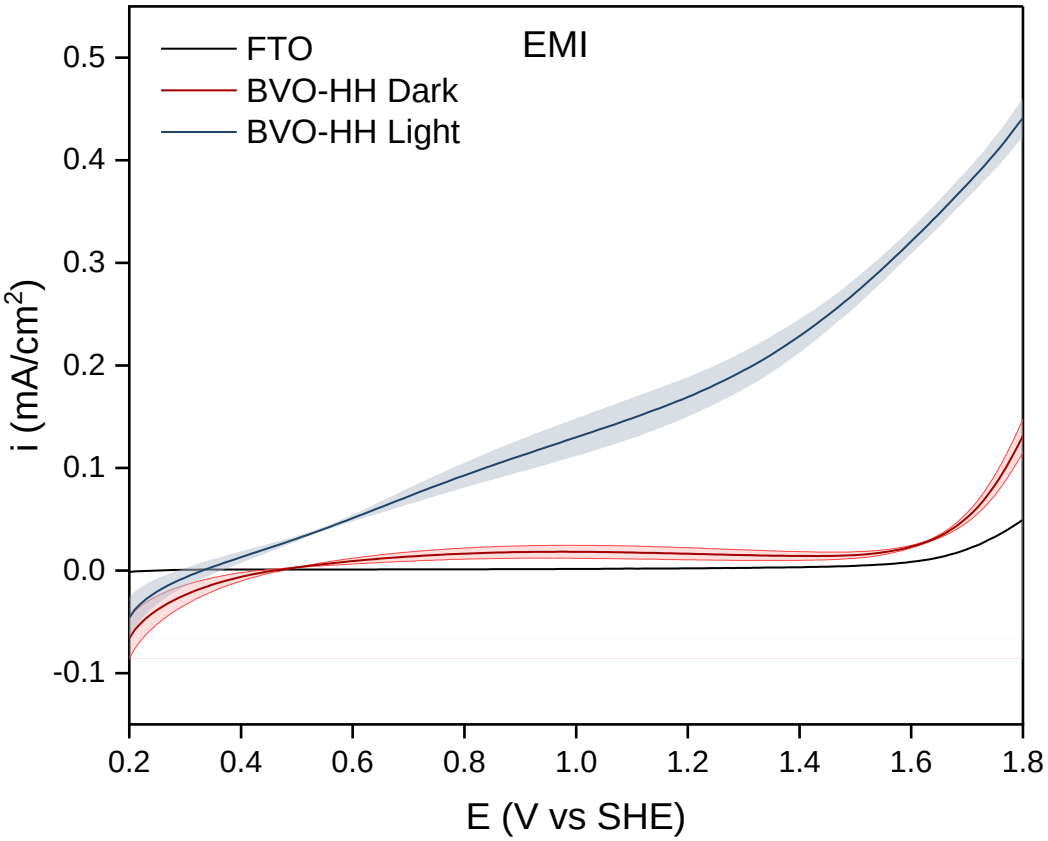

Fig. S3 – LSV analyses under dark and illuminated conditions of the BVO-HH photoanodes produced with the EMI ink. The coloured lines and areas represent the average and interval of confidence obtained with three independent photoanodes.

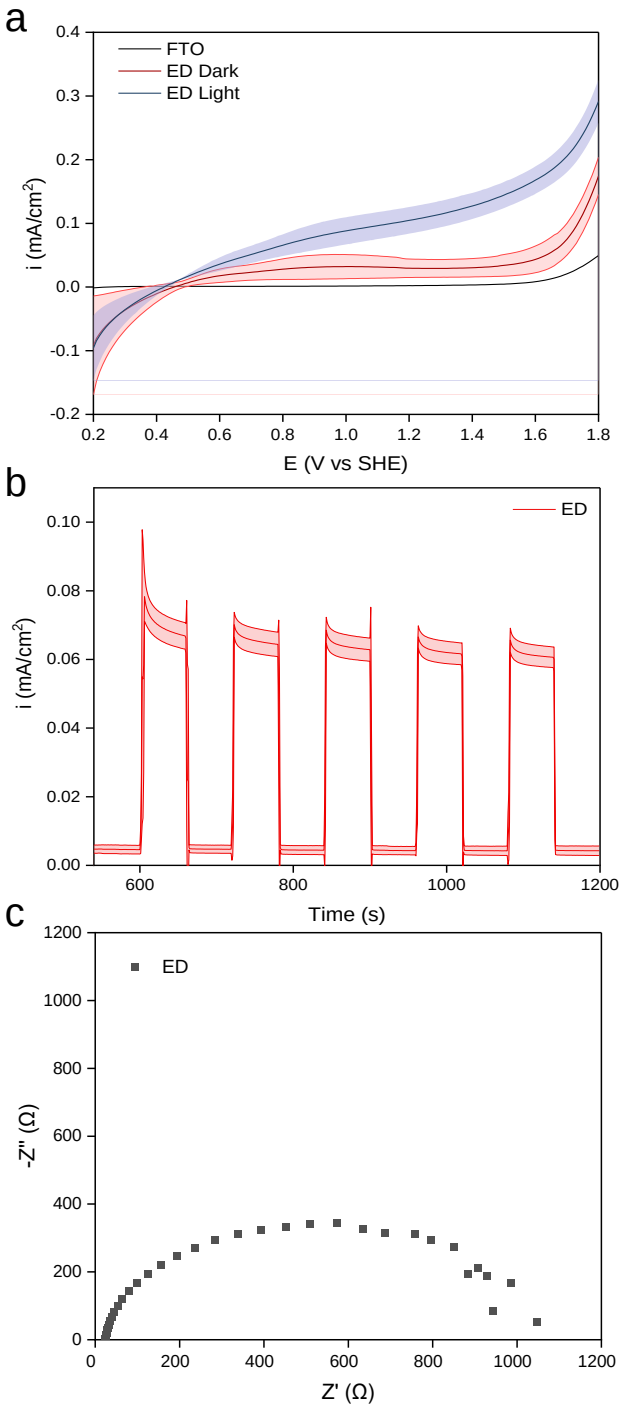

Fig. S4 – (a) LSV analyses of the ED photoanodes under AM1.5G illumination, the coloured lines and areas represent the average and interval of confidence obtained with three independent photoanodes; (b) CA analyses under the intermittent illumination of the ED photoanodes at 1.2 V *vs* SHE bias and AM1.5G illumination; (c) Nyquist plot describing the impedance behaviour of the ED photoanodes under illumination.

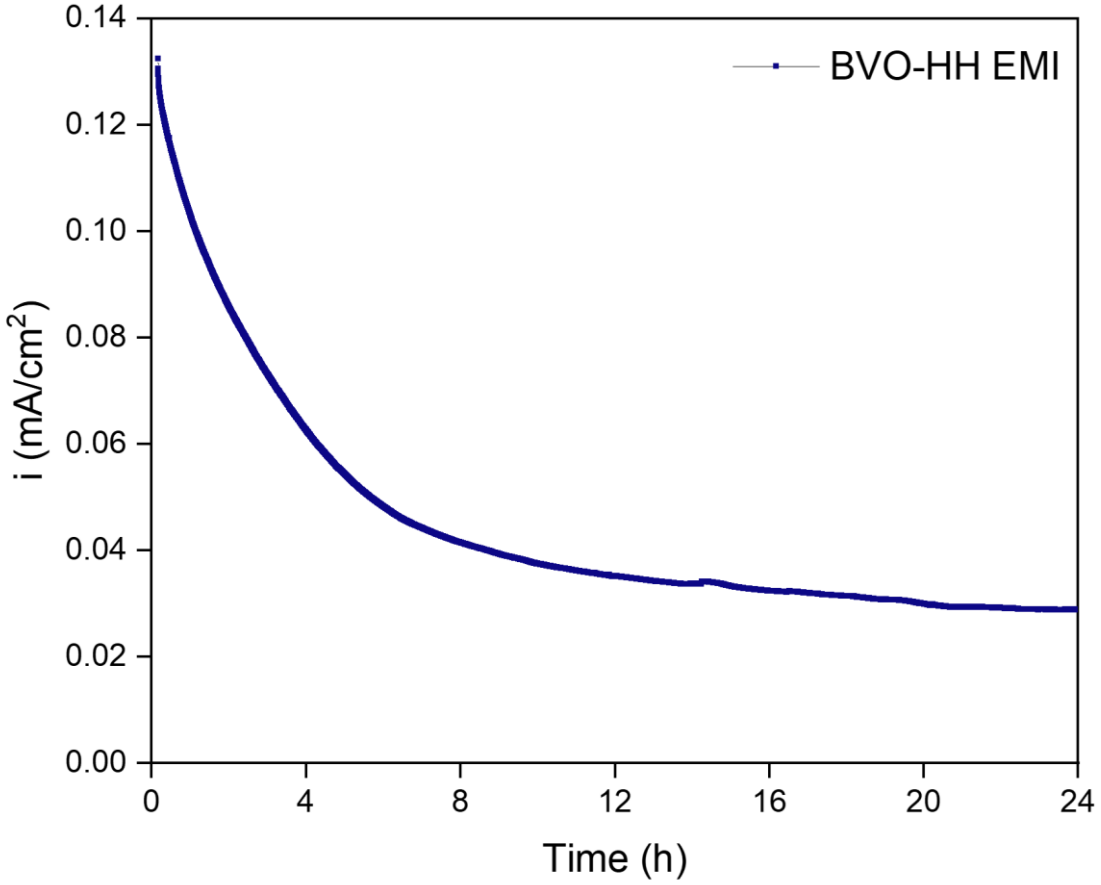

Fig. S5 – Stability test of the BVO-HH EMI photoanode under AM1.5G illumination with phosphate buffer (pH 7.00) at 1.20 V *vs* SHE.

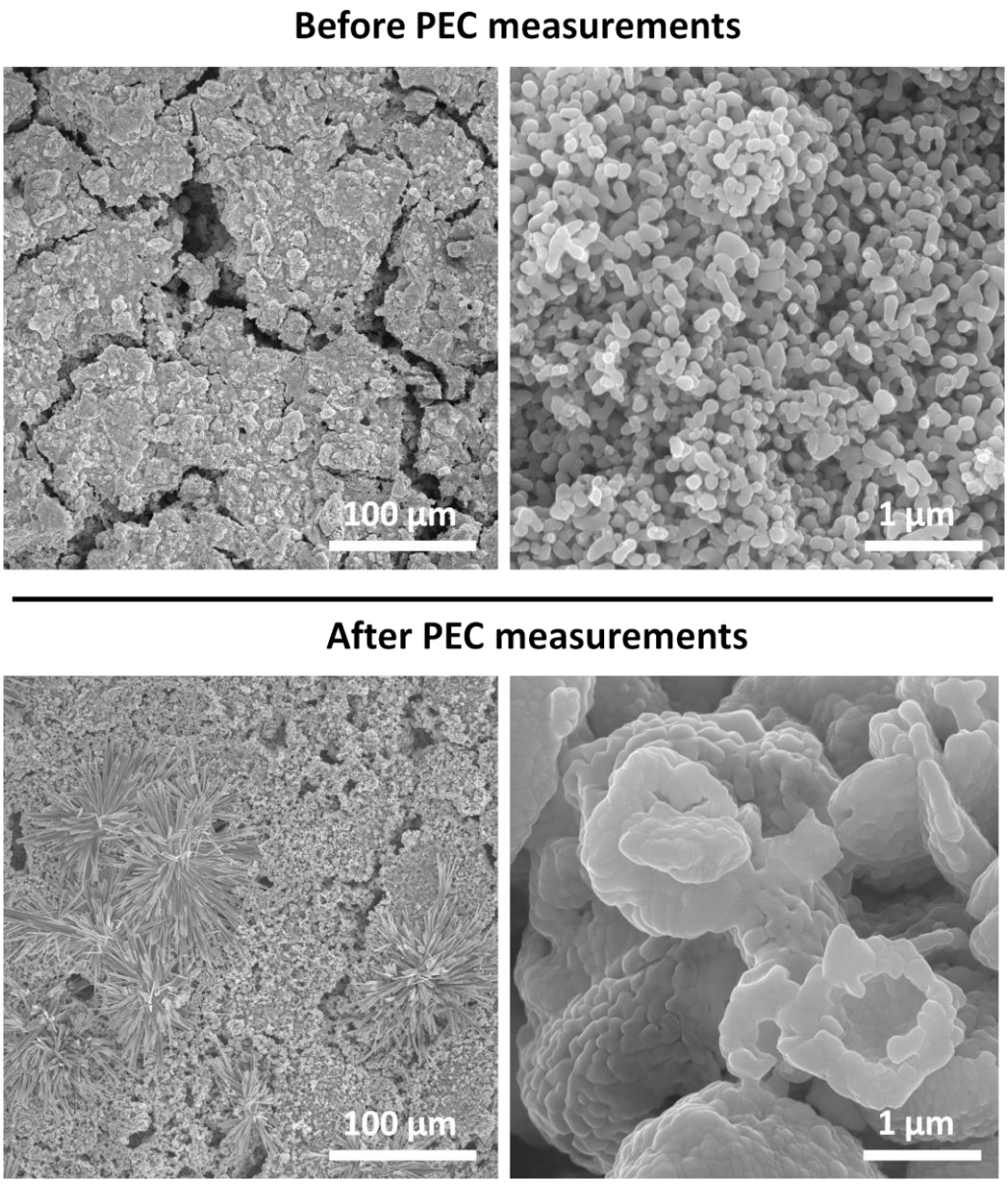

Fig. S6 – SEM images of the BVO slide by electrochemical deposition method before and after PEC measurements.

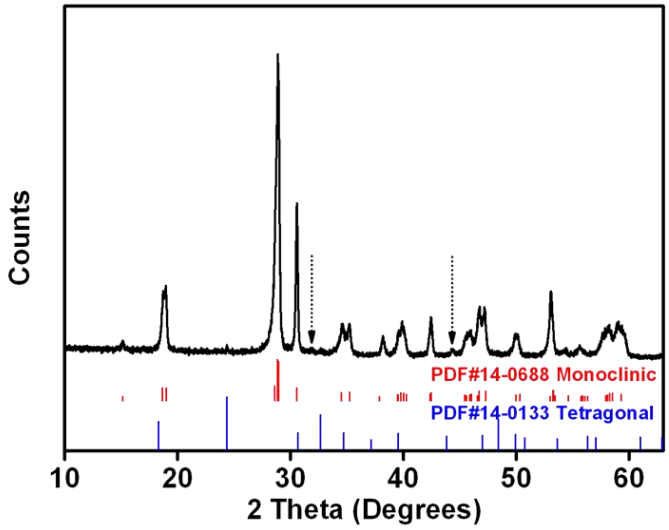

Dinesh_ED_AfterPECMeasurement 1

Element	Mass Norm. [%]	Atom [%]	abs. error [%] (1 sigma)
Oxygen	12.68	64.96	1.52
Vanadium	0.64	1.04	0.05
Bismuth	86.68	34.01	2.20
	100.00	**100.00**	

Fig. S7 – XRD pattern of the $BiVO_4$ powder scratched off the electrochemically deposited BVO slide after PEC measurements. The SEM image and EDX data are for the flower-like structures formed after PEC measurements on the electrochemically deposited BVO slide. The arrows in the XRD graph indicate the diffraction peaks from the impurities.

Doi: 10.1595/205651322X16457018428071

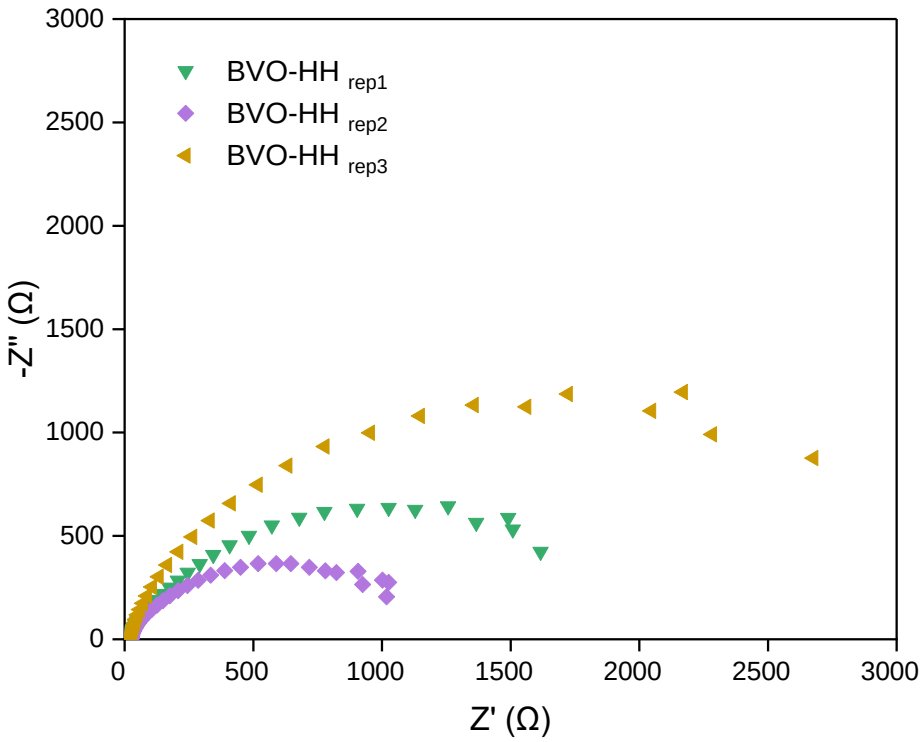

Fig. S8 – Nyquist plot describing the impedance behaviour of the BVO-HH Triton-X photoanodes under illumination.

Doi: 10.1595/205651322X16457018428071

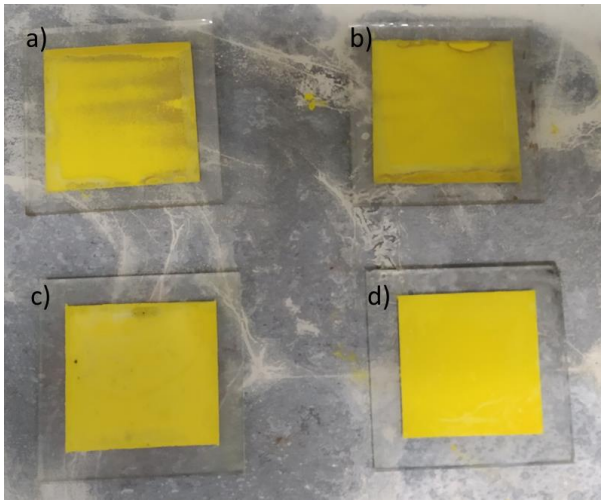

Fig. S9 – $BiVO_4$ photoanodes prepared by electrochemical deposition with varying concentration of vanadyl acetylacetonate calcinated at 450 ^oC. The deposition was accomplished with a uniform coverage of the electrode at a potential of -0.1V *vs* Ag/AgCl (3 M NaCl) under the conditions: a) 0.2 M vanadyl acetylacetonate with temperature ramp rate 5 ^oC/min; b) 0.2 M vanadyl acetylacetonate with ramp rate 2 ^oC/min; c) 0.3 M vanadyl acetylacetonate with ramp rate 5 ^oC/min; and d) 0.4 M vanadyl acetylacetonate with electrode ramp rate 5^oC/min.

Doi: 10.1595/205651322X16457018428071

References

1. B.X. Lei, L.L. Zeng, P. Zhang, Z.F. Sun, W. Sun, & X.X. Zhang. Adv. Powder Technol., 2014, **25**, (3), 946
2. M. Mousavi-Kamazani. J. Mater. Sci. Mater. Electron., 2019, **30**, 17735
3. S. Nikam, & S. Joshi, RSC Adv., 2016, **6**, (109), 107463
4. E.A. Mohamed, Z.N. Zahran, & Y. Naruta. J. Mater. Chem. A, 2017, **5**, (15), 6825
5. A.I. Kontos, A.G. Kontos, D.S. Tsoukleris, M.C. Bernard, N. Spyrellis, & P. Falaras. J. Mater. Process. Technol., 2008, **196**, 243
6. K.R. Tolod, S. Hernández, M. Castellino, F.A. Deorsola, E. Davarpanah, & N. Russo. Int. J. Hydrogen Energ., 2020, **45**, (1), 605.
7. S. Anantharaj, & S. Noda. ChemElectroChem, 2020, **7**, 2297
8. Q. Wang, J. He, Y. Shi, S. Zhang, T. Niu, H. She, & Y. Bi. Chem. Eng. J., 2017, 326, 411-418.
9. M. Arunachalam, Y.J. Seo, S. Jeon, K.S. Ahn, C.S. Kim, & S.H. Kang, S.H. Chem. Eng. J., 2020, 394, 125016.
10. H. She, P. Yue, J. Huang, L. Wang, & Q. Wang. Chem. Eng. J., 2020, 392, 123703.

Doi: 10.1595/205651322X16457018428071